

XMM-Newton observations of the polars EV UMa, RX J1002-19 and RX J1007-20[★]

Gavin Ramsay and Mark Cropper

Mullard Space Science Lab, University College London, Holmbury St. Mary, Dorking, Surrey, RH5 6NT, UK

Received:

ABSTRACT

We present *XMM-Newton* data of three strongly magnetic cataclysmic variables (polars) EV UMa, RX J1002-19 and RX J1007-20. These include the polar with the shortest orbital period (EV UMa) and the polar with one of the highest magnetic field strengths (RX J1007-20). They exhibit a range of X-ray spectral characteristics which are consistent with their known magnetic field strength. We find that two of the systems show evidence for an absorption dip in soft X-rays. Their profiles are well defined, implying that the stream is highly collimated. We determine the mass transfer rate for the two systems with known distances. We determine that the mass of the white dwarf in EV UMa and RX J1007-20 is $\sim 1M_{\odot}$ while in RX J1002-19 it is closer to $\sim 0.5M_{\odot}$.

Key words: Stars: individual: EV UMa, RX J1002-19, RX J1007-20 – Stars: binaries – Stars: cataclysmic variables – X-rays: stars

1 INTRODUCTION

Polars or AM Her systems are accreting binary systems in which material transfers from a dwarf secondary star onto a magnetic ($B \sim 10\text{--}200\text{MG}$) white dwarf through Roche lobe overflow. At some height above the photosphere of the white dwarf a shock forms. Hard X-rays are generated in this post-shock flow (*c.f.* Wu 2000 for a review of the shock structure in these systems). Cyclotron radiation is also emitted in this post-shock flow by electrons spiralling around the magnetic field lines: this radiation is emitted in the optical band. Some fraction of the hard X-rays and cyclotron emission are intercepted by the photosphere of the white dwarf and are re-emitted at lower energies. Soft X-rays can also be produced by dense ‘blobs’ of material which impact directly into the white dwarf.

As part of a programme to determine how the balance of soft and hard X-rays are affected by system parameters such as the magnetic field, we have observed a number of polars using *XMM-Newton*. These include DP Leo, WW Hor (Ramsay et al 2001), BY Cam (Ramsay & Cropper 2002a) and CE Gru (Ramsay & Cropper 2002b). Here, we present the results on three further polars, EV UMa, RX J1002-19 and RX J1007-20, all of which were discovered using

ROSAT. We show their main system parameters in Table 1. These systems show a range of parameters, including the polar with the shortest orbital period (EV UMa), and a polar with one of the highest magnetic field strengths (RX J1007-20). In this paper we first discuss their temporal properties and then their spectral properties.

EV UMa (RE J1307+535) also has exhibited the highest recorded degree of polarisation in any polar (or any astrophysical object for that matter) when the circular polarisation varied from +50 to –20 percent over an orbital cycle when it was in an intermediate accretion state (Hakala et al 1994). The degree of polarisation was reduced when it was at higher accretion states (presumably because of the increased dilution of the polarisation by a bright accretion stream) and the system has a significantly different light curve (Katajainen et al 2000). Although this object has been relatively well observed in the optical and also the EUV (using the Wide Field Camera on *ROSAT*, Osborne et al 1994) no X-ray observations of this object have been published.

RX J1007-20 was shown to show a prominent dip in the soft X-ray light curve, which was attributed to the accretion stream obscuring the emission from one of the accretion sites and also has a very high soft/hard X-ray ratio (Reinsch et al 1999).

Very little information has been published on RX J1002-19.

[★] Based on observations obtained with *XMM-Newton*, an ESA science mission with instruments and contributions directly funded by ESA Member States and the USA (NASA).

Source	Orbital Period	Magnetic field
EV UMa	79.69m ¹	30–40 MG ¹
RX J1002-19	107m ²	
RX J1007-20	208m ²	92MG ³

Table 1. The main system parameters of EV UMa, RX J1002-19 and RX J1007-20. (1) Osborne et al 1994, (2) Beuermann & Burwitz 1995, (3) Reinsch et al 1999.

2 OBSERVATIONS

The satellite *XMM-Newton* was launched in Dec 1999 by the European Space Agency. It has the largest effective area of any X-ray satellite and also has a 30 cm optical/UV telescope (the Optical Monitor, OM: Mason et al 2001) allowing simultaneous X-ray and optical/UV coverage. The EPIC instruments contain imaging detectors covering the energy range 0.1–10keV with moderate spectra resolution. The start time of the EPIC MOS observations preceded the EPIC pn observations. The OM data were taken in one optical band (*V* band) and two UV filters (UVW1: 2400–3400 Å, UVW2: 1800–2400 Å) (in that sequence). The observation log is shown in Table 2. The data obtained using the RGS (den Herder et al 2001) were of low signal-to-noise and are therefore not discussed further.

The data were processed using the *XMM-Newton Science Analysis Software* v5.3. For the EPIC pn detector (Strüder et al 2001), data were extracted using an aperture of 40'' centered on the source. Background data were extracted from a source free region. For the EPIC MOS detectors (Turner et al 2001) we extracted the background from an annulus around the source. The background data were scaled and subtracted from the source data. The OM data were analysed in a similar way using `omichain` and `omfchain` (this latter task was not incorporated into SAS v5.3 but has recently been added to SAS v5.3.3). Data were corrected for background subtraction and coincidence losses (Mason et al 2001). In extracting the EPIC pn spectrum, we used single and double pixel events and used the response files `epn_ff(1w)20_sdY9_thin.rmf` for the full frame and (large window) modes respectively. In the case of the MOS data we used the response files `m[1-2]_thin1v9q19t5r5.all.l15.rsp`.

We show in Table 2 the mean *V* mag determined using the OM for each source at the time of our observation. EV UMa was seen by Osborne et al (1994) in two different brightness levels: *V* = 17–18 and *V* = 20–21. Katajainen et al (2000) found it to be in an even higher accretion state at *V* = 16–17. EV UMa was therefore in a high accretion state during our *XMM-Newton* observations.

RX J1002-19 is quoted as *V* ∼ 17 by Beuermann & Burwitz (1995) and a *ROSAT* PSPC count rate of 0.63 ct/s. Our detection of *V* ∼ 19.6 was made during the X-ray faint phase, so that is probably an underestimate of its mean orbital brightness. However, this together with its mean X-ray brightness (*c.f.* Figure 3) suggests that RX J1002-19 was in an intermediate accretion state.

RX J1007-20 was identified with a *V* ∼ 18 star by Thomas et al (1998) and had a peak *ROSAT* PSPC count rate of ∼ 1 ct/s. This suggests that it was in a similarly high

accretion state at the epoch of the *XMM-Newton* observations.

3 LIGHT CURVES

3.1 EV UMa

3.1.1 XMM-Newton data

Both the EPIC pn and MOS data covered a full orbital cycle. We therefore folded the data from each detector on the orbital period and then binned and co-added them. The X-ray light curve shown in Figure 1 has a prominent bright phase lasting over half the orbital cycle with a broad minimum where the flux is much reduced. In the center of the bright phase there is a prominent dip which is strongest at soft energies: this is characteristic of photo-electric absorption and is due to the accretion stream obscuring the X-rays emitted from one of the accretion regions on the white dwarf. In harder X-rays, the flux after the dip is significantly lower compared to the flux before the dip. We go on to discuss this further below.

Our UVW2 data covers a large fraction of the orbital period (∼ 0.8). We find that it increases in flux at the same phase at the rise to the X-ray bright phase. Unfortunately the data do not cover the phase of the accretion stream dip. After the dip, the flux is around half that of the bright phase before the dip. The *V* band data shows no significant variability, while the short section of UVW1 data shows an initial rise followed by a decline.

3.1.2 ROSAT data

ROSAT made two pointed observations of EV UMa, but on both occasions it was in a low accretion state and not detected. Osborne et al (1994) presents optical photometry and EUV data taken from the *ROSAT* all sky survey using the wide field camera (WFC). The phase-folded optical data shows a basically sinusoidal shape with a secondary minimum (which is most prominent in red light) occurring at what would otherwise be maximum brightness. The WFC S1 filter data (0.09–0.21keV) shows a bright phase lasting ∼ 0.4–0.5 cycles with the remainder being consistent with zero flux: maximum flux coincides with the bright phase in the optical band.

Osborne et al (1994) do not show the *ROSAT* X-ray all sky survey data. We have extracted those data from the archive at MPE and analysed the data using `ftool` procedures and folded the data on the ephemeris of Osborne et al (1994) whose time zero is the maximum of optical pulse. Based on the estimated errors of this ephemeris we expect there to be an uncertainty of 0.05 cycles in the phasing of the *ROSAT* data as in the case of Osborne et al (1994). We show the folded and binned light curve in Figure 2. The light curve shows a marked degree of irregularity. Some of this is probably attributable to that the fact that we have not taken the effects of vignetting into account. However, the light curve clearly shows a broad general variation similar to our *XMM-Newton* data and a narrow dip near $\phi=0.0$. This implies that the secondary minimum in the optical is phased with the general X-ray maximum and the narrow absorption dip at $\phi=0.0$. The EUV data shows no evidence for

	EV UMa	RX J1002-19	RX J1007-20
Date	2001 Dec 8	2001 Dec 10	2001 Dec 7
EPIC MOS	LW thin 7772 sec	FF thin 5992 sec	LW thin 7507 sec
EPIC pn	LW thin 5468 sec	FF thin 3668 sec	LW thin 5203 sec
RGS	8230 sec	6455 sec	7965 sec
OM	Image/fast UVW1 1500 sec	Image/fast UVW1 1500 sec	Image/fast UVW1 1500 sec
OM	Image/fast UVW2 3900 sec	Image/fast UVW2 2000 sec	Image/fast UVW2 3600 sec
OM	Image/fast V 1500 sec	Image/fast V 1500 sec	Image/fast V 1500 sec
Mean <i>V</i> mag	16.6	19.6	18.5
Accretion state	High	Intermediate	High

Table 2. The log of *XMM-Newton* observations of EV UMa, RX J1002-19 and RX J1007-20. LW refers to large window mode and FF full frame mode, while thin refers to the filter used. The exposure time in each detector is shown in seconds. The UVW1 filter has a coverage 2400–3400 Å and UVW2 1800–2400 Å.

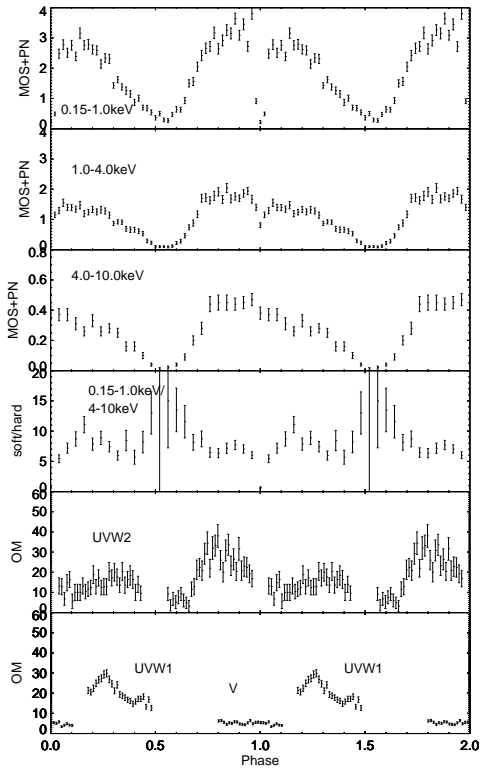


Figure 1. The phased and binned X-ray and optical light curves of EV UMa. We have folded the data on the period of Osborne et al (1994) and defined phase zero as the center of the absorption dip. Energy bands 0.15–1.0keV and 1.0–4.0keV have bin widths of 0.02 cycles, while the energy band 4.0–10.0keV has a bin width of 0.04 cycles. The optical data were binned into 60sec bins (0.012 cycles). The units for the OM data are 10^{-16} ergs s $^{-1}$ cm $^{-2}$.

such an absorption dip, but this may be due to the relatively poor sensitivity of the WFC.

3.1.3 Phasing the optical and X-ray data

We now go on to relate our *XMM-Newton* observations with those made previously and in particular the optical and X-ray light curves. We find that the dip in the *XMM-Newton* data occurs at $\phi=0.65$ on the ephemeris of Osborne et al

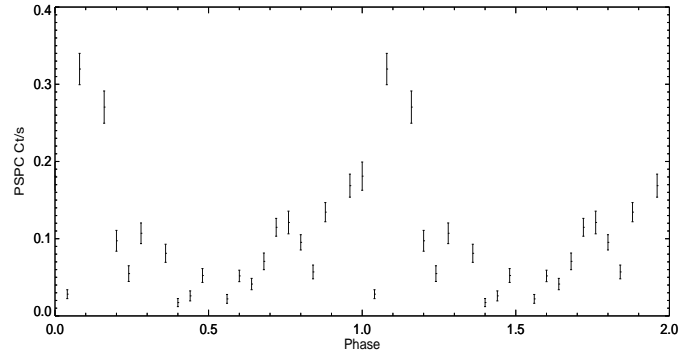


Figure 2. The *ROSAT* all sky survey data of EV UMa folded on the ephemeris of Osborne et al (1994).

(1994) which is based on optical data taken in 1992. The dip seen in the *ROSAT* X-ray light curve (taken in 1990) occurs at $\phi \sim 0.05$ (Figure 2). This implies that the accumulated phase drift between the *ROSAT* and the *XMM-Newton* data is ~ 0.4 cycles.

The Hakala et al (1994) *R* band data (taken in 1994), can therefore be phased such that the positive circular polarisation peak coincides with the absorption dip at $\phi=0.0$ (Figure 1). Also, the data of Katajainen et al (2000) has to be advanced in phase by $\phi \sim 0.2$. This places their narrow dip-like feature in *UBV* bands and the maximum negative circular polarisation (at $\phi \sim 0.20-0.25$ on the ephemeris of Osborne et al 1994) at the same phase as the X-ray dip in our *XMM-Newton* data. Consequently, we find that we expect maximum negative circular polarisation at the phase of maximum brightness whereas Hakala et al found it to be maximally positively polarised. It is possible that there was a reversal in the sign of the polarisation, but it is much more likely that there was an incorrect calibration in either the Hakala et al (1994) or Katajainen et al (2000) data. The data of Hakala et al (1994) were taken using a CCD polarimeter which had an arbitrary beam orientation and there may have been difficulties in determining the correct sign for the circular polarisation (Hakala, priv comm).

Our *XMM-Newton* X-ray data indicate that there is almost a complete absence of X-ray flux at the expected phase at which the secondary accretion region of Hakala et al (1994) would be most prominent. This calls into question the existence of this second region. The high inclination of

this system (Hakala et al 1994) would allow the cyclotron emission from the prime accretion region to be viewed from beneath while the foot-point of the magnetic field was behind the limb of the white dwarf. This could be the explanation for the circular polarisation sign reversal.

Turning to the UV light curves (Figure 1), the low flux levels in the UVW2 data near $\phi \sim 0.6$, and the low X-ray flux, corresponds to the prime accretion region moving behind the limb of the white dwarf. The broad depression around $\phi=0.0$ may be due to the same absorbing material that causes the narrow dip seen in soft X-rays.

3.2 RX J1002-19

The X-ray and optical light curve of RX J1002-19 is shown in Figure 3. This is the first published X-ray light curve of this source. The orbital coverage is almost complete in the MOS instruments ($\Delta\phi \sim 0.9$) with a bright phase lasting $\Delta\phi \sim 0.65$ -0.70 cycles and a faint phase where the flux is essentially zero. This suggests that the accretion region causing the X-ray flux is in the upper hemisphere of the white dwarf.

We also find the presence of a structured dip in the soft X-ray light curve which is not present in the harder band at $\phi \sim 0.18$. This suggests that the dip is due to absorption of X-rays from the accretion region by the accretion stream as found in EV UMa. The UVW1 data shows the appearance of the X-ray region coming into view at the same time as the start of the X-ray bright phase. The flux then decreases around $\phi=0.97$. It is possible that this decrease maybe related to the absorption dip seen in soft X-rays at $\phi \sim 0.18$. The V band data show a low flux level during the faint X-ray phase.

3.3 RX J1007-20

Our X-ray data covers approximately half of the binary orbit (Figure 4). By comparison with both EV UMa and RX J1002-19 the flux in the 1-10keV energy band is very low. In contrast, below 1keV, it is bright and highly variable. The *ROSAT* light curve (Reinsch et al 1999) also shows a variable light curve with a strong dip seen in soft X-rays (no counts at the dip maximum) which they interpreted as an absorption dip similar to that seen in our observations of EV UMa and RX J1002-19. However, such a strong dip is not seen in our data and therefore it is probable that the dip occurred at an orbital phase which we did not observe. (The orbital period is not sufficiently well known to co-phase the *XMM-Newton* data with the archived *ROSAT* data). Reinsch et al (1999) concluded that one pole was visible throughout the orbital cycle although is it close to the limb of the white dwarf at certain phases.

4 X-RAY SPECTRA

4.1 The spectra

In two of the three polars, we extracted spectra from a subset of the available data. In the case of EV UMa (Figure 1) there was some evidence that two distinct emission regions

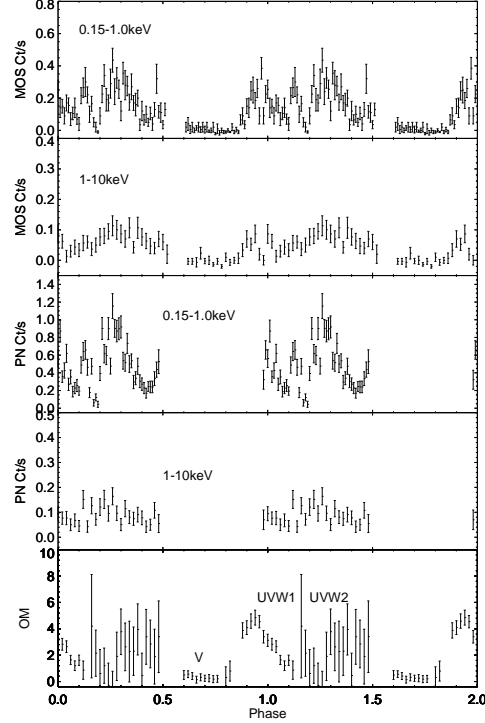


Figure 3. The binned X-ray and OM light curves of RX J1002-19. We fold the data on the orbital period of Beuermann & Burwitz (1995). The phasing is arbitrary. The 0.15–1.0keV data have been binned into 0.01 cycle bins while the 1.0–10.0keV band data and the OM data have been binned into 0.02 cycle bins. The units for the OM data are 10^{-16} ergs s^{-1} cm^{-2} .

are present. We therefore extracted spectra from $\phi=0.70$ –0.95 and $\phi=0.05$ –0.35. These phase ranges excluded the deep absorption dip. For RX J1002-19 we excluded data from the faint phase and also the phase interval which included an absorption dip (centered on $\phi=0.18$, Figure 3). We did not exclude any of the RX J1007-20 data.

We show in Figure 5 the EPIC pn spectra from all three polars. As expected from the low hard X-ray count rate of RX J1007-20 (Figure 4) the spectrum of is dominated by a strong soft X-ray component. Similarly, the strong hard X-ray count rate seen in the light curve of EV UMa is reflected in a prominent hard component (it is much stronger than that of RX J1007-20). The relative strength of the soft and hard components in RX J1002-19 is midway between the other two. There maybe some evidence for line emission near the Fe $K\alpha$ complex in the spectrum of EV UMa but not in RX J1002-19 or RX J1007-20. The absence of such a feature is due to the lower flux and hence lower signal-to-noise ratio in these systems compared to EV UMa.

We define the hard X-ray luminosity as ($L_{hard} = 4\pi\text{Flux}_{hard,bol}d^2$) where $\text{Flux}_{hard,bol}$ is the unabsorbed, bolometric flux from the hard component and d is the distance. Since a fraction of this flux is directed towards the observer, we switch the reflected component to zero after the final fit to determine the intrinsic flux from the optically thin post-shock region (we take into account reflection of hard X-rays from the surface of the white dwarf in our emission model - *c.f.* next section). We define the soft X-ray luminosity as ($L_{soft} = \pi\text{Flux}_{soft,bol}\sec(\theta)d^2$), where we assume that the soft X-ray emission is optically thick and can

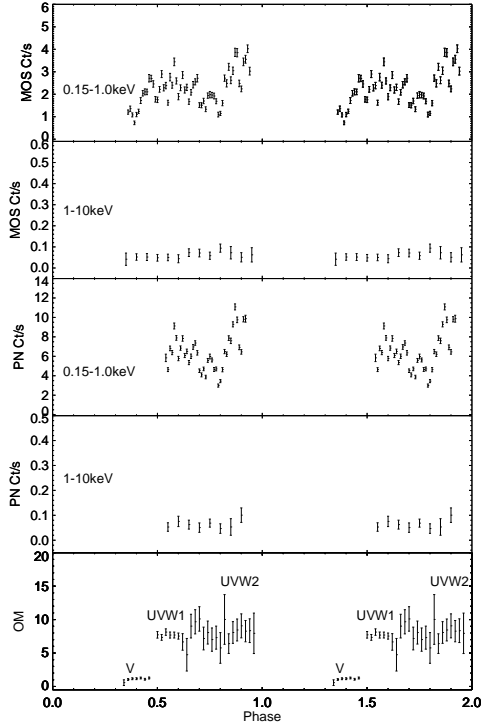


Figure 4. The binned X-ray and OM light curves of RX J1007-20. We fold the data on the orbital period of Beuermann & Reinsch (1995). The phasing is arbitrary. The 0.15–1.0 keV data has been binned into 0.01 cycle bins and the 1.0–10.0 keV data into 0.05 cycle bins. The OM data has been binned into 0.02 cycle bins. The units for the OM data are 10^{-16} ergs s^{-1} cm^{-2} .

be approximated by a small thin slab of material. The unabsorbed bolometric flux is $Flux_{soft,bol}$ and θ is the mean viewing angle to the accretion region. Our emission model of the post-shock region also allows us to estimate the mass of the white dwarf if we assume the white dwarf mass-radius relationship of Nauenberg (1972).

The standard accretion shock model of Lamb & Masters and King & Lasota (1979) suggests that the ratio of the flux from the soft X-ray reprocessed to the post-shock emission should be ~ 0.5 . These values will be a lower estimate since emission from cyclotron emission will contribute to the post-shock luminosity.

4.2 The model

We modelled the data using a simple neutral absorber and an emission model of the kind described by Cropper et al (1999). This emission model, unlike single temperature thermal bremsstrahlung models, is a more realistic physical description of the post-shock accretion region in polars. It is based on the prescription of Aizu (1973) which predicts the temperature and density profiles over the height of the accretion shock. However, it has been modified to take into account cyclotron cooling (which can be significant in polars) and also the variation in gravitational force over the shock height.

To reduce the number of free parameters we fix ϵ_s , (the ratio of cyclotron cooling to thermal bremsstrahlung cooling at the shock front), at a value which implies a magnetic

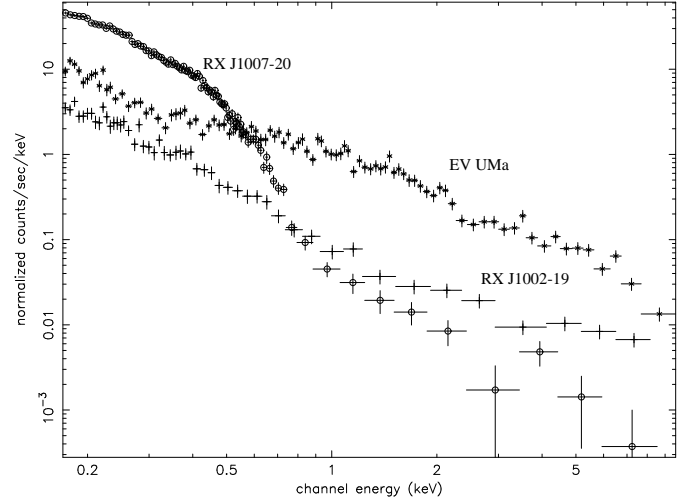


Figure 5. The X-ray spectra of EV UMa, RX J1002-19 and RX J1007-20.

field strength for the polar is question (the magnetic field strength is a function of ϵ_s , mass transfer rate and mass of the white dwarf - *c.f.* equation 2 Wu, Chanmugam & Shaviv 1995).

We also fix the specific accretion rate in the range $1-5$ g s^{-1} cm^{-2} (typical of polars in an intermediate to high accretion state). Changing these parameters does not have a great affect on the results for data with moderate signal-to-noise ratio. We also include reflection of hard X-rays from the surface of the white dwarf using the results of van Teeseling et al (1996). We assume a mean viewing to the reflecting site of 30° . We also added a blackbody model and determined the change in the fit.

4.3 EV UMa

We show the EPIC pn spectrum from $\phi=0.70-0.95$ together with the residuals in Figure 6. Whilst we obtain a reasonably good fit, there is an excess of residuals around $0.5-0.8$ keV. This maybe due to the presence of photoionized line emission which is not accounted for in our emission model. There is no evidence for a significant difference between this spectra and the spectra extracted from $\phi=0.05-0.35$. Further, all EPIC spectra show a low Hydrogen column density ($< 6 \times 10^{19}$ cm^{-2}). The mean viewing angle to the emission region is uncertain. We initially assume a mean viewing angle of 50° . We therefore have to apply a correction factor of $\sec\theta=1.55$ to the blackbody luminosity to take into account that this component is optically thick. EV UMa is one of the most distant polars known: Osborne et al (1994) put a lower limit to the distance of ~ 700 pc and is at least 630 pc above the galactic plane. In determining the luminosities we assumed a distance of 700 pc.

We find that the mass of the white dwarf is reasonably well constrained ($M_{wd} \sim 1.0-1.1 M_\odot$). In fitting the spectra from $\phi=0.05-0.35$ we fix the mass at the values we found from our fits to the spectra extracted from $\phi=0.70-0.95$. Assuming a viewing angle of 50° we find the ratio $L_{soft}/L_{hard} \sim 0.1-0.2$. To increase this ratio so that it matches that predicted by the standard model (Lamb &

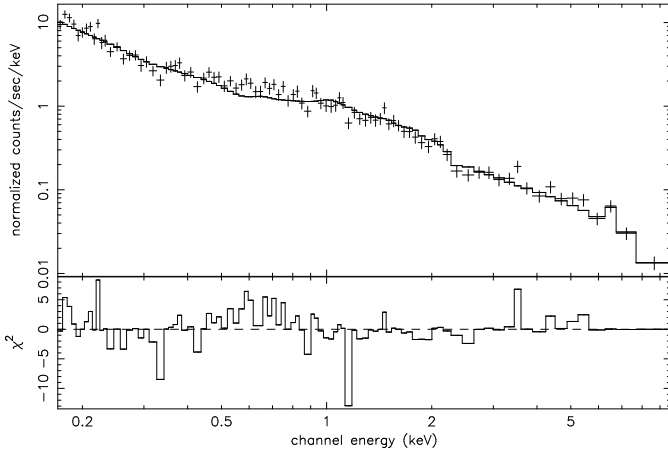


Figure 6. The EPIC pn spectra of EV UMa together with the best fit model and the residuals.

Masters 1979, King & Lasota 1979) we would require a mean viewing angle $\sim 80^\circ$. The Hakala et al (1994) polarisation data modelling predicts that the upper accretion region is seen to rotate into and out from view and hence a high viewing angle is not unreasonable. We suggest in §3.1 that the phase range $\phi=0.05\text{--}0.35$ coincides with the accretion region gradually going behind the limb of the white dwarfs so the viewing angle to this emission site is expected to be even higher than for the previous spectrum.

4.4 RX J1002–19

The EPIC pn spectrum together with the residuals are shown in Figure 7. Similarly to EV UMa, we find an excess of residuals around 0.5–0.7 keV. The spectrum of RX J1002–19 is unusual in that it shows evidence for strong absorption by a neutral absorber with partial covering, (a simple absorber gave significantly poorer fits). The viewing angle to the accretion region is uncertain in this system. However, we do observe it coming over and behind the limb of the white dwarf so the mean viewing angle to the accretion region must be relatively high. We assume a mean viewing angle of 50° giving a correction factor of 1.55 for the reprocessed component. We do not know the distance to this system so we assume a distance of 100 pc in determining the luminosities.

The resulting mass of the white dwarf is not strongly constrained, although the EPIC pn spectrum does indicate that it is less massive than $\sim 1.0 M_\odot$. The MOS spectrum was very poorly constrained so we fixed it at the best fit found from the pn spectrum ($0.5 M_\odot$). In determining the flux of the shocked component we keep the mass fixed. The resulting ratio $L_{\text{soft}}/L_{\text{hard}}$ ($\sim 1\text{--}2$) is slightly greater than expected from the standard shock model. However, if there is a significant cyclotron emission present then this would add to the flux from the shocked component. It would therefore result in a lower ratio which would be close to that expected from the standard shock model.

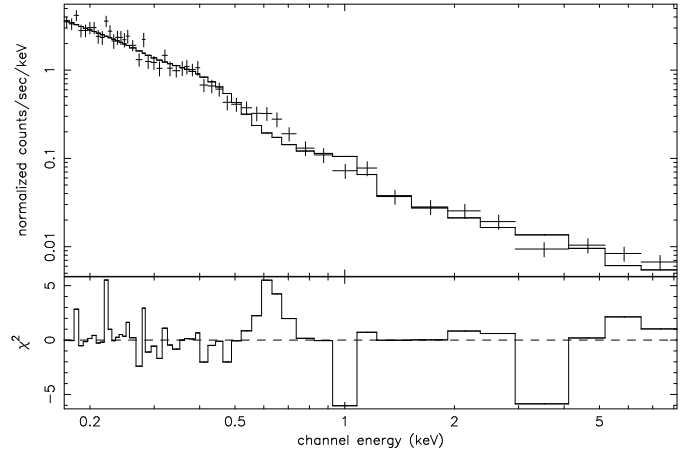


Figure 7. The EPIC pn spectra of RX J1002–19 together with the best fit model and the residuals.

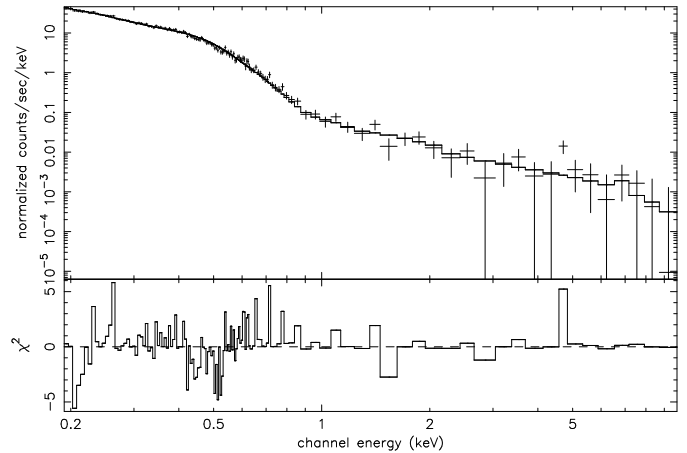


Figure 8. The EPIC pn spectra of RX J1007–20 together with the best fit model and the residuals.

4.5 RX J1007–20

The spectrum of RX J1007–20 is dominated by a strong soft X-ray component. Although the resulting estimate for the mass of the white dwarf is not well constrained, a mass of $\sim 1 M_\odot$ is consistent with both the MOS and pn data. When we determine the flux from the shock component we fix the mass at the best fit value. The viewing angle to the accretion region is uncertain. Therefore, we assume a rather conservative estimate for the viewing angle of 30° giving a correction factor for the reprocessed component of 1.15. In determining the luminosity we assume a distance of 700 pc (Reinsch et al 1999).

The resulting ratio, $L_{\text{soft}}/L_{\text{hard}}$ is ~ 8 and ~ 11 (determined from the pn and MOS detectors respectively) is high: clearly RX J1007–20 has a large ‘soft X-ray excess’. The light curve is highly variable: this is consistent with the view that the soft X-ray excess is due to dense blobs of material which impact the photosphere of the white dwarf directly causing their energy to be re-processed as soft X-rays (Kuijpers & Pringle 1982).

Source	Detector	N_H (10^{20} cm^{-2})	kT_{bb} (eV)	Flux (bb)	$L_{bb,bol}$	Flux (Shock)	$L_{hard,bol}$	$L_{bb,bol}/$ $L_{hard,bol}$	M_{wd} (M_\odot)	χ^2_ν (dof)
EV UMa (1)	PN	$0.0^{+0.6}$	48^{+4}_{-6}	$4.3^{+1.7}_{-0.4}$	98^{+39}_{-10}	13^{+4}_{-7}	735^{+245}_{-196}	$0.13^{+0.12}_{-0.04}$	$1.01^{+0.09}_{-0.08}$	1.82 (89)
EV UMa (1)	MOS	$0.0^{+0.6}$	49^{+7}_{-5}	$3.9^{+1.4}_{-0.8}$	93^{+29}_{-5}	14^{+6}_{-1}	784^{+343}_{-49}	$0.12^{+0.05}_{-0.06}$	$1.09^{+0.07}_{-0.11}$	1.12 (102)
EV UMa (2)	PN	$0.0^{+0.3}$	40^{+4}_{-4}	$6.4^{+2.4}_{-1.1}$	142^{+54}_{-25}	$10^{+0.4}_{-0.4}$	539^{+49}_{-49}	$0.26^{+0.14}_{-0.06}$	1.01 (fix)	1.63 (73)
EV UMa (2)	MOS	$0.0^{+0.5}$	56^{+4}_{-8}	$3.0^{+1.0}_{-0.4}$	64^{+25}_{-10}	10^{+2}_{-2}	588^{+147}_{-98}	$0.11^{+0.08}_{-0.06}$	1.09 (fix)	1.30 (139)
RX J1002-19	PN	480^{+270}_{-130} cf= $0.84^{+0.03}_{-0.03}$	59^{+3}_{-5}	$9.4^{+1.6}_{-1.3}$	$4.3^{+0.8}_{-0.6}$	$2.3^{+0.7}_{-0.5}$	$2.7^{+0.8}_{-0.5}$	$1.6^{+0.8}_{-0.5}$	$0.5^{+0.4}_{-0.1}$	1.41 (45)
RX J1002-19	MOS	330^{+270}_{-120} cf= $0.76^{+0.06}_{-0.07}$	58^{+7}_{-8}	$5.9^{+8.3}_{-0.9}$	$2.8^{+3.8}_{-0.9}$	$1.5^{+0.6}_{-0.4}$	$1.8^{+0.7}_{-0.5}$	$1.6^{+3.6}_{-0.8}$	0.5 (fix)	0.53 (31)
RX J1007-20	PN	$1.10^{+0.25}_{-0.25}$	$61.5^{+2.5}_{-2.0}$	22^{+1}_{-2}	372^{+5}_{-34}	$0.8^{+0.2}_{-0.1}$	47^{+12}_{-6}	$8.1^{+1.4}_{-2.1}$	$1.04^{+0.20}_{-0.32}$	1.17 (125)
RX J1007-20	MOS	$1.3^{+0.4}_{-0.6}$	55^{+2}_{-2}	32^{+5}_{-7}	540^{+50}_{-100}	$0.8^{+0.1}_{-0.1}$	45^{+3}_{-5}	$11.8^{+2.8}_{-2.8}$	$1.05^{+0.12}_{-0.12}$	1.64 (90)

Table 3. The fits to the X-ray data. EV UMa (1) and EV UMa (2) refer to the bright phase before and after the absorption dip – see text for details. For RX J1002-19 we have used a partial covering absorber: ‘cf’ refers to the covering fraction. The blackbody bolometric luminosity, $L_{bb,bol}$ and the X-ray luminosity from post-shock flow, L_{hard} , are defined in the text. The units of flux are 10^{-12} ergs s^{-1} cm^{-2} and luminosity are 10^{30} ergs s^{-1} . We assume a distance to RX J1007-20 and EV UMa of 700pc and 100pc to RX J1002-19.

5 DISCUSSION

We have presented *XMM-Newton* data of three polars, which display rather different characteristics. We find that in each system we cannot obtain good fits to their X-ray spectra using a single component model – they all require a shock model plus a soft blackbody component. However, all three show very different soft/hard X-ray ratios. Further, their light curves show a range of features. We now go on to discuss our findings.

5.1 EV UMa - one or two accretion poles?

The X-ray light curves and the hardness ratio of EV UMa (Figure 1) suggested a different accretion region may dominate before and after the absorption dip. By examining the X-ray spectra from these phase ranges we find that there is no evidence that their spectra differ. Together with the phasing of the X-ray light curves and the optical light curves (§3.1.3) we suggest that there is only one dominant accretion region and the presence of negative circular polarisation for a short time in the optical data of Hakala et al (1994) is due to observing the cyclotron emitting region from beneath.

5.2 Soft/Hard ratio

EV UMa, RX J1002-19 and RX J1007-20 show very different L_{soft}/L_{hard} ratios, with EV UMa showing the lowest and RX J1007-20 the highest. Indeed, RX J1007-20 has a ratio which is a factor of ~ 20 greater than that predicted from the ‘standard’ shock model of Lamb & Masters (1979) and King & Lasota (1979). However, the fact that it has a high magnetic field strength (92 MG, Reinsch et al 1999), a large ‘soft X-ray excess’ is consistent with the work of Ramsay et al (1994) and Beuermann & Burwitz (1995) who showed that this ratio was correlated with magnetic field strength; with high field systems showing high soft/hard ratios. To account for this, the most likely solution is that dense blobs of material impact with the white dwarf directly without forming a shock (Kuijpers & Pringle 1982) or the shock is buried

sufficiently deep for the bremsstrahlung emission to be thermalized in the local photosphere of the white dwarf (Frank, King & Lasota 1988). The fact that we observe strong flaring activity in the light curve of RX J1007-20 is consistent with this view.

Based on the soft/hard ratio we predict that RX J1002-19 will have a magnetic field strength which is slightly greater than that of EV UMa. If we observe the accretion region(s) of EV UMa at a high viewing angle then its soft/hard ratio is consistent with the standard shock model.

Ramsay et al (2001) showed that using a single temperature thermal bremsstrahlung model for the hard X-ray component rather than a stratified shock as used here, the resulting ratio L_{soft}/L_{hard} is higher: in the case of DP Leo by a factor of 2. This should be taken into account when comparing with studies using single temperature models.

5.3 Masses

We can infer the mass of the white dwarf from our model fitting assuming a mass-radius relationship for the white dwarf. Using the Nauenberg (1972) relationship we find that both EV UMa and RX J1007-20 have masses of $\sim 1M_\odot$. In the case of RX J1002-19 the mass is not very well constrained, although it is likely to be less than $1M_\odot$ with a best fit of $0.5M_\odot$.

Using the same model for the shock region as here, Ramsay (2000) fitted *RXTE* spectra from 21 mCVs and found that their masses were biased towards higher masses than that of isolated white dwarfs. There was no significant difference between the mass of the white dwarf in mCVs and non-magnetic CVs. This is consistent with the masses reported here and also the other mCVs which have been observed using *XMM-Newton*: CE Gru ($\sim 1.0M_\odot$, Ramsay & Cropper 2002b), BY Cam ($0.9\text{--}1.1M_\odot$, Ramsay & Cropper 2002a), DP Leo ($>1.3M_\odot$, Ramsay et al 2001) and WW Hor ($\sim 1.0\text{--}1.1M_\odot$, Ramsay et al 2001). It remains to be seen whether there is a systematic bias in the masses determined with this method using *XMM-Newton* data.

5.4 Mass transfer rate

To determine the mass transfer rate we use the standard relation, $L_{acc} = GM_{wd}\dot{M}/R_{wd}$. The accretion luminosity, L_{acc} , is the sum of L_{hard} , the unprocessed fraction of the cyclotron luminosity, L_{cyc} , and the luminosity of any dense blobs of material which do not form a shock and emit in soft X-rays. We use the best fit masses determined from our model fits to determine the mass accretion rate for EV UMa and RX J1007–20 (we omit RX J1002–19 since there is no estimate for its distance).

In the case of EV UMa, the results of our spectral analysis indicate there is no evidence for blobby accretion. Using the model results of Woelk & Beuermann (1996) and assuming a magnetic field strength of (30–40MG) and a mass $M_{wd}=1.0M_{\odot}$, we find $L_{cyc}/L_{hard} \sim 1$ –10 for a range of $\dot{m}=1$ –10 g cm^{−2} s^{−1}. This implies $L_{cyc} = 7.5$ – 70×10^{32} ergs s^{−1}. The mass transfer rate is therefore ~ 6 – 30×10^{15} g s^{−1} and hence the fraction of the white dwarf that is accreting is ~ 1.6 – 8.3×10^{-3} .

In the case of RX J1007–20 the spectral results indicate that a significant proportion of the soft X-ray luminosity is in the form of blobby accretion. We therefore include L_{soft} when determining the total luminosity. We again use the model results of Woelk & Beuermann (1996) to estimate L_{cyc} and assume $B=92$ MG and $M_{wd}=1.0M_{\odot}$. We find that $L_{cyc} \sim 10$ – $100 \times (L_{hard} + L_{soft})$ and hence $L_{cyc} \sim 4$ – 50×10^{33} ergs s^{−1}. This implies $\dot{M} \sim 2$ – 20×10^{16} g s^{−1} and a fractional area of ~ 5 – 60×10^{-3} .

It is difficult to compare these mass transfer rates with previous results because of the different way authors account for the cyclotron flux and whether they include the soft X-ray luminosity. However, the fractional area of the white dwarf which is accreting is consistent with previous studies.

5.5 Absorption dips

Absorption dips of the kind seen in EV UMa and RX J1002–19 are caused by the accretion stream obscuring the emission sites on the white dwarf as it passes through our line of sight. For an accretion region in the upper hemisphere of the white dwarf, such a dip is inevitable if the latitude of the region, m , is less than the binary inclination, i . In the case of EV UMa, Hakala et al (1994) finds the optical polarisation data is best modelled with a high inclination ($\sim 75^\circ$) so it is likely that this condition holds. The inclination for J1002–19 is currently unknown. The dip ingress and egress in EV UMa is rapid: the ingress takes 20–30 sec and less than 20 sec for the egress (Figure 9). Such a rapid ingress and egress imply that the stream is highly collimated. For RX J1002–19 the dip structure is more complex (Figure 9) with a shorter dip preceding the main dip which also has a sharp profile.

The dip duration (defined as the full width half maximum of the dip profile) is 0.057 and 0.042 cycles for EV UMa and RX J1002–19 respectively (where we do not include the shorter dip). Using equation (14) of Watson et al (1989) we find that for the observed duration of the dips, $r_s = 0.18d$ and $0.13d$ for EV UMa and RX J1002–19 respectively where r_s is the radius of the accretion stream and d is the distance between the white dwarf and the source which is causing the absorption dip. (We assume the stream is in

the orbital plane). For a stream radius of 10^9 cm these radii imply $d = 5.5 \times 10^9$ and 7.7×10^9 cm.

To make a very approximate estimate of the radius at which the accretion stream becomes coupled by the magnetic field, R_{μ} , we use equation (1b) of Mukai (1988). If we use the best fit masses, the mass accretion rates determined in §5.4, the radius of the accretion stream, $r = 1 \times 10^9$ cm, and $B=30$ MG we derive $R_{\mu} = 1.1 \times 10^{10}$ and 3.5×10^{10} cm for EV UMa and RX J1002–19. Although there is a great deal of uncertainty in some of the values of these parameters and the applicability of equation (1b) of Mukai (1988), it does suggest that the stream which is obscuring the accretion region during the dip is located in the magnetically controlled portion of the accretion flow.

We can make an estimate of the total column density of the stream by taking our best model fits then increasing the absorption until the model count rate matches the observed count rate at dip maximum for the specified energy range. We find a column density of 7 – 20×10^{22} cm^{−2} and $\sim 1 \times 10^{21}$ cm^{−2} for EV UMa and RX J1002–19 respectively. We can make an estimate of the number density of the stream using equation (6) of Watson et al (1995). Assuming the accretion flow is in the orbital plane and using the above values of the total column density we find $n_{13}r_9=5$ and 0.05 for EV UMa and RX J1002–19 respectively, where n_{13} is the constant number density in units of 10^{13} cm^{−3} and r_9 is the radius of the stream in units of 10^9 cm. For comparison Watson et al (1995) found $n_{13}r_9=5$ for RX J1940–10. Taking these values at face value, they imply that either the accretion stream in RX J1002–19 has a rather small radius or a low number density.

6 ACKNOWLEDGMENTS

We acknowledge the use of the *ROSAT* all-sky survey data archive held at MPE, Garching, Germany.

REFERENCES

- Aizu, K., 1973, *Prog Theor Phys*, 49, 1184
- Beuermann, K., Burwitz, V., 1995, *ASP Conf Series*, Vol 85, 99
- Cropper, M., Wu, K., Ramsay, G., Kocabiyyik, A., 1999, *MNRAS*, 306, 684
- den Herder, J. W., et al, 2001, *A&A*, 365, L7
- Done, C., Osborne, J. P., Beardmore, A. P., 1995, *MNRAS*, 276, 483
- Frank, J., King, A. R., Lasota, J. -P., 1988, *A&A*, 193, 113
- Hakala, P. J., Pirola, V., Vilhu, O., Osborne, J. P., Hannikainen, D. C., 1994, *MNRAS*, 271, L41
- Ishida, M., Matsuzaki, K., Fujimoto, R., Mukai, K., Osborne, J. P., 1997, *MNRAS*, 287, 651
- Katajainen, S., Lehto, H. J., Pirola, V., Karttunen, H., Piironen, J., 2000, *A&A*, 357, 677
- King, A. R., Lasota, J. P., 1979, *MNRAS*, 188, 653
- Kuijpers, J., Pringle, J. E., 1982, *A&A*, 114, L4
- Lamb, D. Q., Masters, A. R., 1979, *ApJ*, 234, 117
- Mason, K. O., et al 2001, *A&A*, 365, L36
- Mukai K., 1988, *MNRAS*, 232, 135
- Nauenberg, M., 1972, *ApJ*, 175, 417
- Osborne, J. P., Beardmore, A. P., Wheatley, P. J., Hakala, P., Watson, M. G., Mason, K. O., Hassall, B. J. M., King, A. R., 1994, *MNRAS*, 270, 650

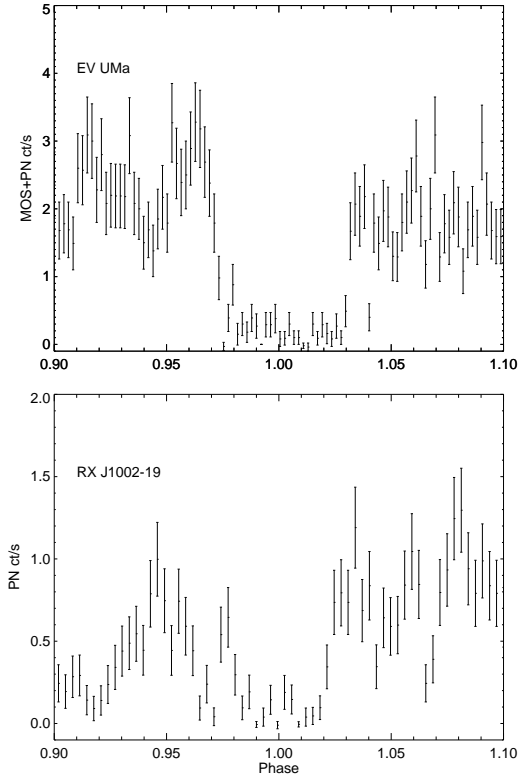


Figure 9. The EPIC pn X-ray light curves (0.15–1.0keV) of EV UMa and RX J1002-19 showing the accretion stream dip in detail. The integration time is 10 and 20 sec for EV UMa and RX J1002-19 respectively. We have phased the light curves so that phase 0.0 corresponds to the centre of the dip.

- Patterson, J., 1984, *ApJS*, 54, 443
 Ramsay, G., Mason, K. O., Cropper, M., Watson, M. G., Clayton, K. L., 1994, *MNRAS*, 270, 692
 Ramsay, G., 2000, *MNRAS*, 314, 403
 Ramsay, G., Cropper, M., Cordova, F., Mason, K., Much, R., Pandel, D., Shirey, R., 2001, *MNRAS*, 326, L27
 Ramsay, G., Cropper, M., 2002a, accepted, *MNRAS*
 Ramsay, G., Cropper, M., 2002b, accepted, *MNRAS*
 Reinsch, K., Burwitz, V., Beuermann, K., Thomas, H. -C., 1999, *ASP Conf Series*, Vol 157, 187
 Strüder, L., et al, 2001, 365, L18
 Thomas, H.-C., Beuermann, K.; Reinsch, K., Schwöpe, A. D., Truemper, J., Voges, W., 1998, *A&A*, 355, 467
 Turner, M., et al 2001, *A&A*, 365, L27
 van Teeseling, A., Kaastra, J. S., Heise, J., 1996, *A&A*, 312, 186
 Watson, M. G., King, A. R., Jones, M. H., Motch, C., 1989, 237, 299
 Watson, M. G., et al, 1995, *MNRAS*, 273, 681
 Woelk, U., Beuermann, K., 1996, *A&A*, 306, 232
 Wu, K., Channugam, G., Shaviv, G., 1995, *ApJ*, 455, 260
 Wu, K., 2000, *Space Science Reviews*, 93, 611